Soft Matter

PAPER

View Article Online
View Journal | View Issue

Cite this: *Soft Matter*, 2025, **21**, 2258

The effect of cholesterol on the bending modulus of DOPC bilayers: re-analysis of NSE data†

Frank Heinrich *[ab] and John F. Nagle *[a]

Received 6th November 2024,
Accepted 18th February 2025

DOI: 10.1039/d4sm01312c

rsc.li/soft-matter-journal

The effect of cholesterol on the bending modulus K_C of DOPC lipid bilayers has been controversial. Previous analysis of dynamic neutron spin echo (NSE) data reported that 50% cholesterol increased K_C by a factor of three in contrast to earlier studies using four different static methods that reported essentially no increase. We reanalyzed the previous NSE data using new developments in NSE analysis. We find that the same NSE data require non-zero viscosity in pure DOPC and they are consistent with no increases in K_C with cholesterol. Instead, we find more than a five-fold increase in the membrane viscosity η_m. We have further added diffusional softening dynamical theory to the basic phenomenological model. This generally decreases the 5-fold increase in viscosity, but the NSE data are not sufficient to determine by how much.

1 Introduction

Biomembranes generally are mechanically flexible, thereby facilitating shape changes in biological functions. Mammalian membranes have many lipid components, including cholesterol. The conventional wisdom of twenty years ago was that cholesterol stiffened membranes. This was based on its effect on lipid bilayers composed of lipids with saturated hydrocarbon chains. Adding cholesterol thickens such bilayers by straightening the hydrocarbon chains, and it increases the bending modulus K_C, which is an important measure of mechanical flexibility. In contrast, about fifteen years ago it was found that, while cholesterol conformed to the conventional wisdom for saturated chains,[1,2] it did not increase K_C of bilayers of lipids with unsaturated chains,[1–5] thereby maintaining membrane flexibility while allowing the incorporation of cholesterol, which is also necessary for mammalian biological function.

In contrast, more recent work using neutron spin echo (NSE) reported that cholesterol increases K_C of the di-unsaturated lipid DOPC substantially by a factor of three with 50% cholesterol.[6] A new theoretical development in NSE data analysis provides the opportunity to address this discrepancy as it considers the influence of membrane viscosity η_m on the small vesicles employed in these studies.[7] Using this updated model, we have re-analyzed the NSE data,[6] also including the effect of vesicle diffusion that was previously neglected. Our re-analysis aligns with earlier findings[2–5] indicating that K_C of DOPC lipid bilayers does not increase with the addition of cholesterol. According to our phenomenological analysis, the slowing down of the NSE data with cholesterol is instead due to an increase in viscosity η_m.

The concept of diffusional softening is becoming central for discussing the bending modulus of lipid bilayers consisting of mixtures of lipids on a more fundamental level.[8–12] Accordingly, we have extended our analysis to include a recent dynamical theory of diffusional softening,[11] modified for NSE samples, and find that it readily fits the NSE data with no increase in K_C with added cholesterol. However, the NSE data do not extend to long enough times to distinguish between different ways of incorporating diffusional softening.

Section 2 reviews the pertinent equations in the phenomenological model and how these parameters affect the underlying dynamics. Section 3 visualizes the data, which is important for applying a correction for the diffusion of the vesicles in the NSE sample. Section 4 presents the results of fitting the NSE data to the basic phenomenological model, and Section 5 extends the analysis to include diffusional softening. Discussion ensues in Section 6.

2 Spherical dynamics model

Starting from the Helfrich–Canham free energy, the thermally averaged mean square equilibrium amplitude $\langle h_l^2 \rangle$ of the l_m spherical harmonic mode of the membrane undulations of a vesicle of radius R under zero tension is[7]

$$\langle h_l^2 \rangle = \frac{k_B T}{K_C} \frac{R^2}{(l+2)(l-1)l(l+1)}, \quad (1)$$

[a] *Department of Physics, Carnegie Mellon University, 5000 Forbes Ave., Pittsburgh, PA 15213, USA. E-mail: fheinrich@cmu.edu, nagle@cmu.edu*
[b] *Center for Neutron Research, National Institute of Standards and Technology, Gaithersburg, MD 20899, USA*

† Electronic supplementary information (ESI) available. See DOI: https://doi.org/10.1039/d4sm01312c

independently of m, so the total roughness is

$$\langle h^2\rangle = \frac{1}{4\pi}\sum_{l=2}^{l_{max}}(2l+1)\langle h_l^2\rangle = \frac{R^2}{12\pi}\frac{k_BT}{K_C} \quad (2)$$

where the last equality is for the limit of large l_{max}.

The new development[7] recognizes that, dynamically, the modal relaxation rates are affected by the membrane viscosity, according to

$$\omega_l = \frac{K_C(l-1)l^2(l+1)^2(l+2)}{\eta_w R^3(4l^3+6l^2-1)+\eta_m R^2(4l^2+4l-8)}, \quad (3)$$

where η_w is the viscosity of water and η_m is the membrane viscosity. Then the autocorrelation functions for the undulations are

$$\langle h_l(t)h_l(0)\rangle = \langle h_l^2\rangle e^{-\omega_l t} \quad (4)$$

A commonly used expression for the neutron spin echo intermediate structure factor $S(q,t)$ is[7,13]

$$S(q,t)/S(q,0) \simeq \exp[-q^2\langle\Delta h^2(t)\rangle]\exp(-q^2Dt) \quad (5)$$

where q is the magnitude of the NSE scattering vector. The first factor in eqn (5) is obtained from the thermally averaged mean square differences in undulation positions after an initial time[7]

$$\langle\Delta h^2(t)\rangle = \frac{1}{4\pi}\sum_{l=2}^{l_{max}}(2l+1)\left\langle|h_l|^2\right\rangle(1-e^{-\omega_l t}). \quad (6)$$

The last factor in eqn (5) is widely accepted to account for diffusion of the vesicles.[7,13–17]

The first factor in eqn (5) is an approximation[7] that could be improved upon, but with little numerical difference, as we have verified. We also note that eqn (5) assumes that the neutron beam is laterally coherent over the diameter of the vesicles. Corrections for typical coherence lengths of 20 nm or more are quite small for vesicles of radius 30 nm pertinent to this paper.

It is illuminating to look at calculations for pertinent values of the parameters. Calculations of $S(q,t)$ are q dependent but

$$-\frac{1}{q^2}\ln[S(q,t)/S(q,0)] = \langle\Delta h^2(t)\rangle + Dt \quad (7)$$

is not q dependent, and it relates more directly to the dynamical properties of the vesicles on the right-hand side of this equation. The thick solid lines in Fig. 1 show the time evolution of the undulations alone $\langle\Delta h^2(t)\rangle$, setting D = 0 in eqn (7). The upper solid blue curve is for zero membrane viscosity, and the lower solid green curve is for a typical membrane viscosity η_m of 1 nano Pa m s. At long times, both curves saturate to the equilibrium membrane roughness given by eqn (2). Comparing them shows that membrane viscosity η_m slows the dynamics considerably. The dotted lines in Fig. 1 show pertinent power laws that are expected to hold before saturation. The curve with viscosity has an extended range from 5 to 500 ns during which the expected $t^{1/2}$ power law[7] is followed before saturation sets in. At shorter times, $\langle\Delta h^2(t)\rangle$ falls below the power law line because the number of modes l_{max} is limited due to the in-plane molecular granularity of lipid molecules. An estimate of

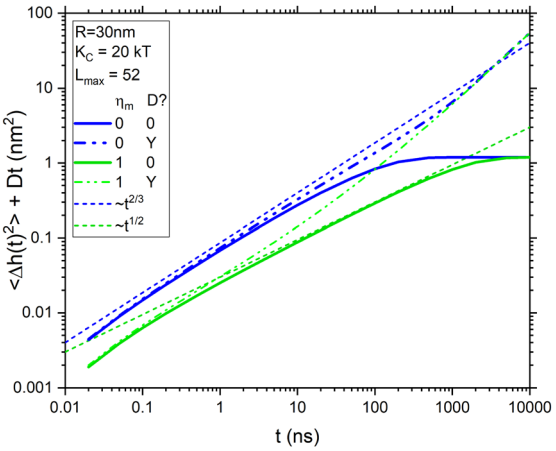

Fig. 1 Dynamics from eqn (7) that illustrate the effect of viscosity (blue *vs.* green) and diffusion (solid *vs.* dash–dot–dot) for a fixed value of K_C = 20 kT and 52 modes for R = 30 nm, compared to two power laws (dotted). The radius used for diffusion is 42 nm and the viscosity units are nPa s m.

the effective in-plane spacing of 1.8 nm from X-ray diffuse scattering[18] gives l_{max} = 52. Similarly, the curve without viscosity also deviates from the Zilman–Granek (ZG) $t^{2/3}$ power law[19] at short times, but it also deviates more quickly at longer times due to faster saturation.

Fig. 1 also shows dash–dot–dot curves for the total displacements sensed by NSE by adding Dt for vesicle diffusion, where D in water was calculated from the Stokes–Einstein equation. The curve for η_m = 0 appears to follow the ZG $t^{2/3}$ power law to much later times. However, by 100 ns, it has already reached a value that exceeds the saturation limit set by eqn (2). In contrast, the total NSE curve with non-zero viscosity never follows the $t^{1/2}$ power law, but it could be construed to follow the ZG $t^{2/3}$ power law in limited time ranges. In either case, these curves emphasize that diffusion has to be considered in analyzing data. The most direct way to do that is to correct for vesicle diffusion by dividing out the last factor in eqn (5) from $S(q,t)$ data.

3 Data visualization

Although it is typical for NSE papers to show $S(q,t)/S(q,0)$ curves for a dozen q values on the same plot, it is more illuminating to plot the left-hand side of eqn (7) as shown for the NSE data for DOPC[6] in Fig. 2. (The typical plots are shown in ESI† and the TOC figure.) The data were reported for eight values of q in the range 0.339 nm^{-1} to 0.682 nm^{-1} with times from 0.657 ns to 100 ns.[6] The $S(q,t)$ for three of the q values did not extend over the full time range. The other five were averaged and shown in Fig. 2 as upward-pointing triangles. There were also four values of q in the range 0.729 nm to 1.01 nm^{-1} with times from 0.871 ns to 45.1 ns for three of these, and their averages are shown by downward pointing triangles in Fig. 2. See page 2 of ESI† for more details.

To apply the diffusion correction, the coefficient of diffusion of the vesicles was calculated from the Stokes–Einstein equation using an appropriate vesicle radius. The vesicles were

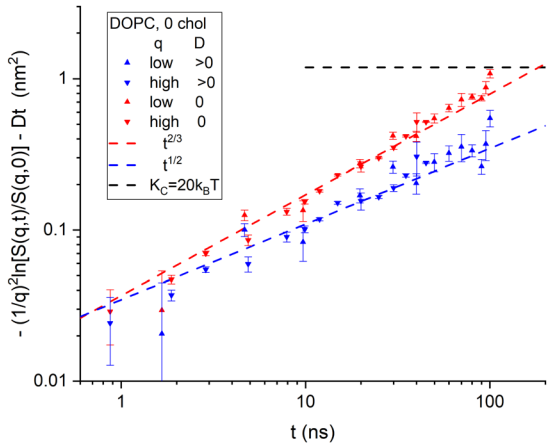

Fig. 2 Log–log plot of the time dependence of NSE data[6] binned into low q and high q ranges. No diffusion correction was made for the data labeled in the legend by $D = 0$. A diffusion correction using a radius of 42 nm was made for the same data and labeled $D > 0$ in the legend. The horizontal dashed line shows the value given by eqn (2) for $K_C = 20$ kT. Uncertainties, here and throughout the manuscript, represent one standard deviation.

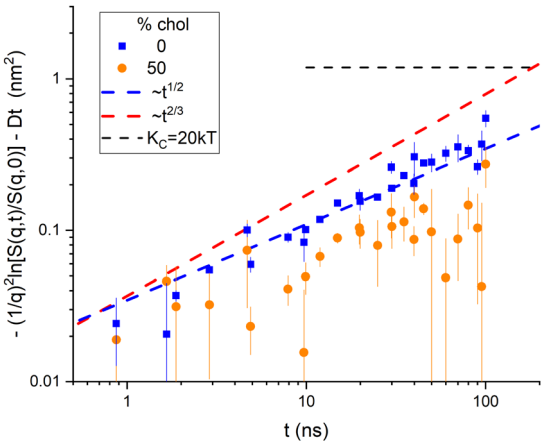

Fig. 3 Comparison of the binned diffusion corrected 50% cholesterol data with the 0% data.

reported to have been extruded with a standard 50 nm diameter filter.[6] Although no direct measurement of the actual size was reported,[6] another recent study using the same filter size and extruder model reported 30 nm radii,[7] and earlier studies have reported similar values.[20] One expects a larger effective radius for vesicle diffusion that includes the edge of the outer monolayer and any immobilized water. Also, interactions between neighboring vesicles decrease their mobility,[16] which is taken into account by increasing the radius. We used a diffusional radius of 42 nm that was also recently reported using dynamic light scattering while using the reported 30 nm from SANS analysis[7] for the undulational radius for the theory in Section 2.

Fig. 2 reiterates the point in Fig. 1 that taking vesicle diffusion into account, as we do above makes a major difference. Doing so, Fig. 2 clearly indicates membrane viscosity in the data because the log–log slope is close to 1/2. On the other hand, if it is supposed that vesicle diffusion should not be taken into account, as appears to have been the case in the previous analysis,[6] then extrapolation of the data to long times would exceed the level shown by the horizontal dashed curve in Fig. 2. That level is given by eqn (2) and the long-time, static, equilibrium value of K_C. To raise that level sufficiently would require, noting that Fig. 2 is a log plot, using considerably smaller values of K_C and/or larger values of R.

We finish this visualization of the data by comparing 50% cholesterol with 0% in Fig. 3. Although the high cholesterol data are much noisier, it is clear that the time course is slower, and it seems closer to a 1/2 power than to a 2/3 power.

What this section has done is to re-emphasize that a correction for vesicle diffusion is essential[16,17] even for pure DOPC before any consideration of cholesterol. Furthermore, a correction based on a diffusion radius of 42 nm for the Stokes estimate of D is reasonable. We have also tried using the SANS radius of 30 nm for the diffusion correction, but it leads to these plots failing to approach saturation and even decreasing at the longest times, which is inconsistent with the relaxation of the undulation modes, as shown in Fig. S4 (ESI†). This preliminary analysis is, therefore, helpful to the detailed fitting of the $S(q,t)$ data to which we turn next.

4 Fitting the data

While the perspective in the preceding section is revealing, there is no substitute for fitting the $S(q,t)/S(q,0)$ data to the model in Section 2. Although the main physical quantities of interest in the model are the membrane viscosity η_m and the bending modulus K_C, let us first explain the choices we made for other parameters that also affect the fits. The data have a normalization factor $S(q,0)$ in eqn (5) for each q.[17] Accordingly, we have here allowed $S(q,0)$ to rescale to best fit the data. Rescaling typically amounted to less than 2% deviation from unity, which hardly affects the data at long times but may alleviate noisy short time $S(q,t)/S(q,0)$ values that often exceed unity. As mentioned, the number of modes also affects the noisy short-time data. After fitting with different numbers of modes, no substantial differences emerged, so we have chosen $L_{max} = 52$ as already mentioned. Extruded unilamellar vesicles also have a distribution of radii with dispersions of order 30%.[7] However, calculations that had this degree of polydispersity differ negligibly from those that simply use the mean radius of 30 nm, so a polydispersity parameter was not used.

The data[6] include uncertainties for each q and t, which were used to calculate the total reduced χ^2 and $\chi^2(q)$ for each q. A recent NSE analysis excluded low q data,[7] but the $\chi^2(q)$ values here were rather random for the different q and cholesterol concentrations, so we have included all twelve q values in our simultaneous fitting of the parameters. However, we have not included in our figures the results from the fits to the 40% cholesterol data because they had considerably larger χ^2, the values of the parameters were out of line with the monotonic sequence of values from the other concentrations, and the 40% data had different time and q values.

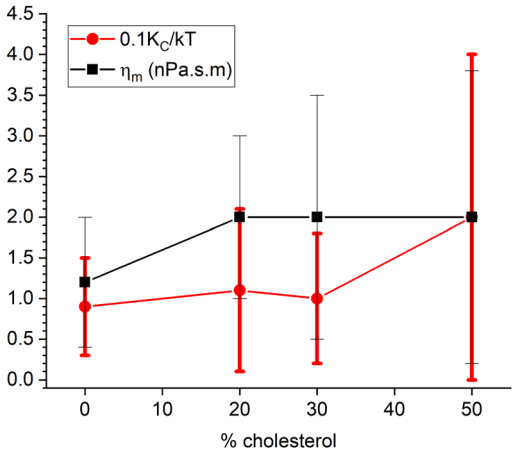

Fig. 4 Results of fitting both K_C and η_m.

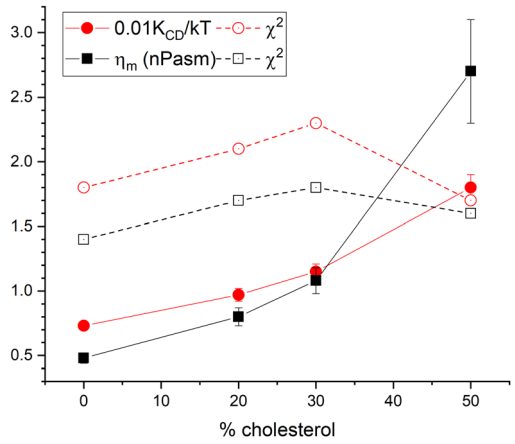

Fig. 6 Filled symbols show results of fitting either to K_{CD} (circles) with η_m fixed to 0 or to η_m (squares) with K_C/kT fixed to 20. Open symbols show the corresponding reduced χ^2.

Ideally, one would like to obtain both K_C and η_m by fitting the data. Our attempt to do this is shown in Fig. 4. Although one might discern an increase in both K_C and η_m, the uncertainties in the parameters are about as large as their best values. The underlying reason is that increases in both parameters have similar effects on $S(q,t)$ as shown in Fig. 5. Therefore, the uncertainties in these parameters are highly correlated, and it is essentially impossible to disentangle reliable values. Basically, the data are too noisy to obtain valid numbers for both parameters.

However, the data are good enough to fit one parameter when the other is held fixed. Fig. 6 shows our results. The filled circles show the values for the bending modulus when the viscosity η_m was set to 0. This is labeled K_{CD} in the legend because it is conceptually similar to what was done earlier,[6] as explained in Section 6.1. Even with no cholesterol, this K_{CD} is much larger than the static value of K_C, and it increases by a factor of 2.5 for 50% cholesterol, similarly to what was earlier reported.[6] In contrast, the black squares in Fig. 6 show the result of fitting the data when K_C/kT was fixed to 20, consistent with the static value.[2] In this case, the viscosity η_m increases by over a factor of 5 for 50% cholesterol. The χ^2 plots in Fig. 6 show that the latter fit is better for all cholesterol concentrations, thereby suggesting that the better model for the effect of cholesterol on NSE data is a constant K_C and increasing η_m. ESI† shows traditional $S(q,t)$ figures with detailed statistics.

Fig. 7 compares the time evolution of $\langle \Delta h^2(t) \rangle$ of the two models to each other and to the experimental NSE data. Both models fit the NSE data reasonably well in its available time window. NSE alone would be a better discriminator of the two models if it had a longer time window or if the lipid more quickly approached its long time limit. However, it is not necessary to use NSE alone because the long time limit in Fig. 7 is given by the equilibrium static bending modulus using eqn (2). The value $K_C/kT \approx 20$ that everyone agrees on when there is no cholesterol in DOPC gives the long time limit of the model with non-zero η_m in Fig. 7 whereas the $\eta_m = 0$ model shown by the red line has $\langle \Delta h^2(\infty) \rangle$ that is far smaller than what is required by eqn (2). Therefore, for the two extant models, only the one with viscosity accommodates the data for both time scales.

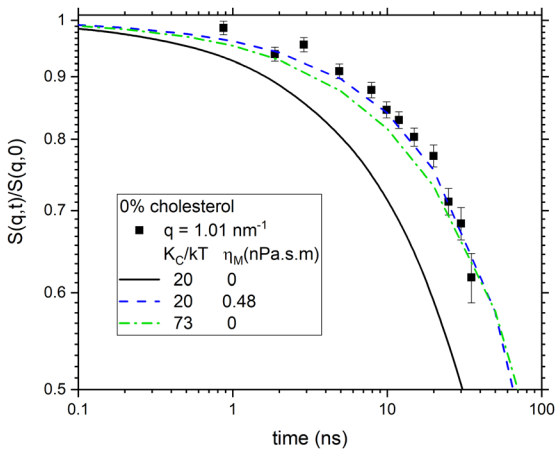

Fig. 5 Comparison of the effect of increasing K_C and η_m on $S(q,t)$. For clarity only one q value is shown.

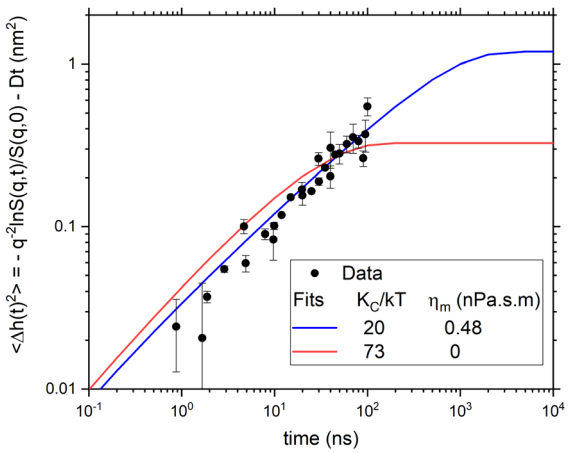

Fig. 7 Comparison of the two salient models to the averaged experimental data in Fig. 3 for DOPC with no cholesterol.

The difference between the 30 nm structural radius and the 42 nm diffusional radius seems rather large. Along with the 30 nm radius, a second structural radius of 40.3 nm has been given that used a different analysis.[16] We have also fit the data with this larger structural radius. This does not change the main conclusions. In particular, the χ^2 are almost unchanged. The fitted η_m and K_{CD}/kT become larger. For no cholesterol, the 0.48 nPa s m in Fig. 7 becomes 0.88 nPa s m, and the 73 for K_{CD}/kT becomes 116. Detailed results are given in Fig. S2(6) and S2(8) in ESI.†

5 Lateral lipid diffusional softening

The concept of diffusional softening is central for discussing the bending modulus of lipid bilayers consisting of mixtures of lipids.[8–12] The title of this section emphasizes that the diffusion involved is that of lipids within the bilayer and not the diffusion of the vesicles in the NSE experiments that we focused on earlier. Briefly, thermally excited undulations create local regions of curvature to which lipids of similar spontaneous curvature diffuse, exchanging with lipids of dissimilar spontaneous curvature that diffuse to undulational regions of the opposite curvature; this couples lateral diffusion and undulations, enabling further curvature and reducing the bending modulus. For two lipids, each with the same value of K_C in their single component bilayers, straightforward equilibrium theory obtains a decrease in the modulus of the mixture that is proportional to the square of the difference ΔC_0 in their effective spontaneous curvatures.[11] There is not yet experimental confirmation for mixtures of two lipids that each alone has the same K_C value, and there is no derivation when the individual K_C have different values. In any case, for cholesterol, there is the experimental problem that pure cholesterol does not form bilayers.

Importantly, a dynamical theory of diffusional softening has been developed and applied to the dynamics of giant unilamellar vesicles of POPC/DOPE (GUVs) with radii of order 10 μm.[11] Like cholesterol mixtures, that system also has no pure DOPE endpoint, so the dynamical theory was necessary to detect diffusional softening. Let us see how this theory might apply to the effect of cholesterol on much smaller NSE vesicles. The first difference compared to the theory in Section 2 is that the coupling of diffusion and undulations leads to two rate constants $k_{l,\pm}$ for the decay of each mode l of the autocorrelation function

$$\langle h_l(t)h_l(0)\rangle = (1-\alpha)\cdot\exp(-tk_{l,+}) + \alpha\cdot\exp(-tk_{l,-}), \quad (8)$$

where α is given by

$$\alpha = \frac{A_{chol}(\Delta C_0)^2\chi(1-\chi)\kappa}{2kT}\frac{(l-1)(l+2)}{l(l+1)}, \quad (9)$$

where A_{chol} is the area of a cholesterol molecule in the bilayer, ΔC_0 is the difference in spontaneous curvatures of DOPC and cholesterol, χ is the area fraction of cholesterol for a given mole fraction and κ is related to the measured static equilibrium bending modulus K_C by

$$\kappa = K_C/(1-\alpha). \quad (10)$$

Adding cholesterol increases $k_{l,+}$ (note the sign error in eqn (36) in that paper[11]) by α times $D_0 l(l+1)/R^2$; this latter diffusion factor for a typical coefficient of lipid, not vesicle, lateral diffusion[21,22] D_0 of 10^{-7} cm^2 s^{-1} is only about (15 000 ns)$^{-1}$ for the largest $l = 2$ mode, so $k_{l,+}$ in eqn (8) is hardly affected by the coupling to diffusion. The $k_{l,-}$ rate in eqn (8) is $1-\alpha$ times the same lateral diffusion factor; it is much slower than $k_{l,+}$, so qualitatively, this slows down $\langle\Delta h^2(t)\rangle$ as cholesterol is added. Most importantly, the increase in the amplitude of this slow rate and the decrease in the amplitude of the fast rate in eqn (8) slows down the overall decay of the autocorrelation function.

It is first important to appreciate that there is a problem with this theory, as written,[11] that is revealed by applying it to zero cholesterol. Then, the $k_{l,+}$ used in eqn (8) is the same as ω_l in eqn (3) when η_m is set to zero and the slow term in eqn (8) doesn't matter because α is zero, so the fit to the NSE data gives the same result as our $\eta_m = 0$ model that gives the red curve in Fig. 7. There it was emphasized that this contradicts the static, equilibrium value of $K_C/kT \approx 20$ when there is no cholesterol. What appears to be missing from the diffusional softening dynamic theory is membrane viscosity. It is fine to ignore η_m in eqn (3) for GUVs until η_m becomes very large[23] because the second term in the denominator of eqn (3) is small compared to the first term. For DOPC, the ratio of those terms is less than 0.1, even for the lowest $l = 2$ mode. But this is not so for smaller NSE vesicles.

We have taken diffusional softening into account in fitting the NSE data in two ways. Both ways use $A_{chol} = 0.35$ nm^2 and $A_{DOPC} = 0.70$ nm^2 to obtain the area fractions χ. Although the dominant mode is $l = 2$, we follow precedent by using the ratio of the l factors to be unity.[11] We have also fixed the coefficient of lipid lateral diffusion D_0 to 3×10^{-8} cm^2 s^{-1} as a typical value from other experiments.[21] Finally, we continue to fix K_C/kT to 20 to match the long-time equilibrium value. In the first way, we have used an estimate of $\Delta C_0 = 0.481$ nm^{-1} (Alex Sodt, private communication) and a similar value of 0.401 nm^{-1} can be obtained from the literature.[24] Combining eqn (10) with eqn (9) gives a quadratic equation that determines the α values shown by the upward pointing triangles in Fig. 8. Fitting used the autocorrelation functions in eqn (8) with $k_{l,+}$ amended to include viscosity as in eqn (3). Fig. 8 shows that η_m increases with increasing cholesterol, but only about half as much compared to Fig. 6 where diffusional softening was not included. This comparison would imply that the effect of cholesterol on NSE dynamics is about half due to increasing viscosity and about half due to lipid diffusion.

In our second way to include diffusional softening, we fit the diffusional α parameter in eqn (9) while holding K_C and η_m fixed. (As before, NSE data are only good enough to fit one parameter.) Results are shown in Fig. 9. The spontaneous curvature difference ΔC_0 is larger than estimated in the first way above, and it decreases from 0.68 nm^{-1} to 0.57 nm^{-1} as cholesterol concentration increases from 20% to 50%. Importantly, χ^2 is practically the same as it is in Fig. 8, and both are

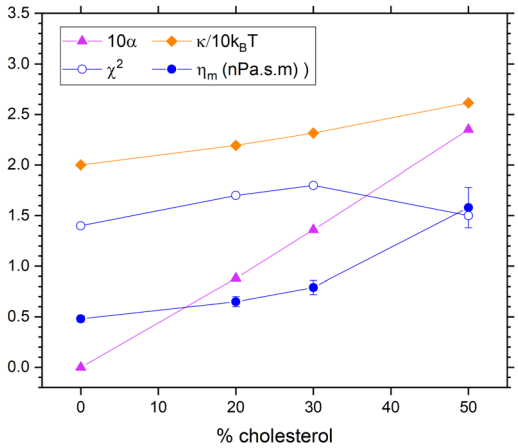

Fig. 8 Results that include dynamical diffusional softening theory in fits to the NSE data using an estimate ΔC_0 = 0.481 nm^{-1} for the spontaneous curvature difference. The estimated values of α (times 10, upward triangles) were used to fit the data resulting in the membrane viscosity (circles) and the unsoftened κ obtained from eqn (10).

the same as for the case shown in Fig. 6 by black squares that has viscosity and no diffusional softening.

6 Discussion

6.1 Fuller discussion of differences with original analysis of these data

The earlier analysis[6] relied on three foundations. The first employed the Zilman–Granek theory[19] for flat plaquettes which gave $t^{2/3}$ power law behavior for $\langle \Delta h^2(t) \rangle$. However, for many years, the viscosity of water η_w had to be chosen three times larger than the actual value in order to obtain reasonable values of K_C.[25]

The second foundation alleviated that problem by a theory[26] that included membrane viscosity and found that what is measured in the NSE experimental regime was a dynamic K_{CD} modulus which satisfied

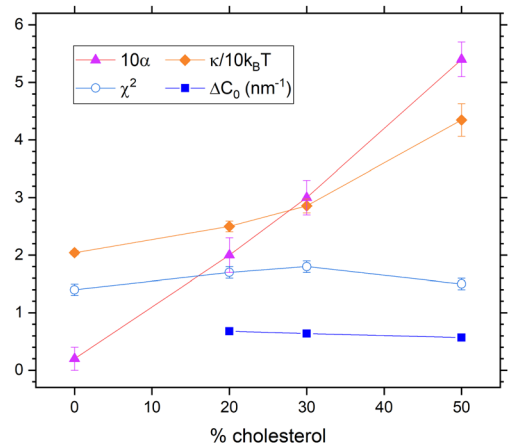

Fig. 9 Results that include dynamical diffusional softening theory in fits that constrained η_m to its value with no cholesterol. The obtained values of α (times 10, upward triangles) were used to fit the data resulting in the membrane viscosity (circles) and the unsoftened κ obtained from eqn (10).

$$K_{CD} = K_C + h^2 K_A \quad (11)$$

where K_A is the area compressibility modulus and h is the distance from the center of the bilayer to either monolayer neutral surface where no excess stress occurs upon bending.[26,27] It has been noted that eqn (11) would provide a way for NSE to experimentally measure the neutral surface h in bilayers using other techniques to measure K_A and K_C.[28] For each undulational wavenumber l this theory splits the dynamical response into two relaxation modes. The faster one gives rise to the K_{CD} modulus which includes both the equilibrium bending modulus K_C and the h^2K_A term that plays a similar role to viscosity in the theory in Section 2. The slower mode would then account for changing the red η_m = 0 curve in Fig. 7 at long times to agree with the equilibrium K_C. The slower mode is usually estimated to be important only at times longer than NSE data.[26] While this general theory has been discussed for spherical vesicles,[29] it has only been implemented for NSE analysis for flat plaquettes.[26]

The third foundation was to employ the polymer brush relation

$$K_A = 24K_C/(2D_C)^2 \quad (12)$$

where D_C is the thickness of the monolayer hydrocarbon region. Previous criticism[28,30] of the earlier NSE analysis[6] focused on this third foundation because the polymer brush model was based on freely jointed chains and the rigid ring structure of cholesterol is not jointed at all. Therefore, the polymer brush model[31] was deemed inadequate for cholesterol, and a replacement theory provided by Evans gave no increase in K_C of DOPC with increasing cholesterol.[2]

6.2 Moving forward

It recently became apparent that the first foundation for NSE data analysis of biomembranes employed in many NSE papers is flawed. While the Zilman–Granek theory of flat plaquettes has usually been assumed, the typical NSE systems have been unilamellar vesicles. This distinction and its likely importance to NSE analysis was discussed earlier.[32] It has been shown more recently for POPC/POPS (90/10) vesicles that it does indeed matter greatly how shape is taken into account.[7] Using all three foundations in the preceding subsection resulted in values of K_{CD} and K_C an order of magnitude too large. In contrast, replacing the traditional Zilman–Granek formula in the first foundation with the spherical model in Section 2 resulted in acceptable values of K_{CD} assuming that eqn (11) in the second foundation remains valid. That paper also emphasized that it is very important to take vesicle diffusion into account;[7] not doing so apparently accounts for why some earlier papers had been able to obtain sensibly smaller values of the bending moduli using the Zilman–Granek theory of flat plaquettes.[6,33]

That recent paper[7] only presented results assuming η_m = 0, in order to focus on the shape issue by comparing to the original Zilman–Granek flat plaquette theory that also had no membrane viscosity.[19] We have also analyzed the POPC/POPS data in that paper and, similar to our results for the DOPC/cholesterol data, we find smaller χ^2 when K_C is constrained to

the experimental 26 kT of POPC[34] and η_m is allowed to fit. We obtain 0.8 nPa s m, compared to our 0.48 nPa s m for DOPC with no cholesterol in Fig. 6.

The analysis for spherical vesicles outlined in Section 2 conceptually bypasses the second and third foundations of the original analysis[6] discussed in the previous subsection. Although the data are not good enough to obtain both K_C and η_m, we propose that the way forward is to constrain K_C to values obtained from other experiments and use NSE to find the best value for the viscosity. It would be especially relevant to do NSE experiments on DMPC where the equilibrium values of K_C increase dramatically with added cholesterol.[2] We predict that the best fit would have an increase in both viscosity and K_C.

However, a casualty of this proposal is that it loses the handle on the determination of the neutral surface h in bilayers *via* eqn (11). Since the χ^2 values are not very much higher in Fig. 6, would it be legitimate to invoke eqn (11) as an alternative way to take into account the viscosity? If it were, then using the values of K_{CD} in Fig. 6 and the values of K_A and K_C from the literature[2] in eqn (11) gives values of h/D_C to be 0.66, 0.65 and 0.57 for 0%, 30% and 50% cholesterol, respectively. The ratio for DOPC is close to the value 0.65 obtainable from a simulation that reported h at 0.94 nm (ref. 35) and the experimental D_C at 1.44 nm.[36] These values of h/D are rather smaller than the value of unity often assumed.[6] Even if we use R = 40 nm, h/D_C is only 0.88 for DOPC. The decrease in h/D_C with cholesterol towards the center of its rigid rings also seems intuitively plausible. For comparison, our analysis of the POPC/POPS data[7] gives h/D_C = 0.75 for R = 30 nm. It might also be mentioned that a finite lateral compressibility $1/K_A$ is central to this approach, whereas the theory in Section 2 assumes zero compressibility. Therefore, further theoretical development has been called for[23] that might allow for using NSE to obtain the neutral surface and maybe provide better fits to NSE data.

6.3 Perspectives

The first perspective of the dynamical theory in Section 2 is that a lipid bilayer has a single bending modulus embodied in the Helfrich–Canham theory for the free energy of undulations. The H–C theory has no dynamics, so the conventional bending modulus pertains to the free energy required to perform a static deformation, as measured by electrodeformation[3] and tether pulling[4,5] experiments. It also pertains to the thermally induced average mean square $\langle h_i^2 \rangle$ in eqn (2) measured by shape fluctuations[3] and X-ray diffuse scattering.[2] These equilibrium measurements obtain the traditional H–C bending modulus K_C that has no time or length scale dependence. A refinement recognizes that the H–C free energy is a continuum theory that should be modified to include tilt and a tilt modulus K_t that become important at short length scales,[37] including the shorter ends of both X-ray diffuse scattering and NSE length scales. Although this has only been taken into account in the analysis of X-ray data,[18,38] it is small enough that it is not likely to be a major concern for the broader issues regarding NSE analysis that we address here. Interestingly, re-analysis of the original X-ray data[2] shows that the tilt modulus increases with cholesterol, as shown in Fig. (S3) (ESI†), and this may be connected with NMR data,[6] as discussed earlier.[28]

The second perspective of the dynamical theory in Section 2 is that adding a single linear transport property, namely membrane viscosity η_m, suffices to describe undulational dynamics through the time-dependent relaxation of spontaneous or imposed fluctuations, such as for the autocorrelation function in eqn (4). Viscosity is a traditional quantity for characterizing time-dependent material properties of soft matter. Of course, this perspective recognizes that short-time, high-frequency responses are attenuated, such as in dielectrics. Likewise, for an overdamped spring, there is a single modulus, the spring constant, while the dynamics vary with the viscosity, both internal, analogous to η_m, and external, analogous to water viscosity η_w. It would seem that this latter perspective is more fundamental than just invoking a frequency/time-dependent modulus. It also allows for predictions for relaxation time regimes that have not yet been measured.

It may be interesting to speculate on why the viscosity might increase with cholesterol. Cholesterol increases the bilayer thickness and the lateral chain packing order parameter and decreases the area per lipid,[2] Hence, the hydrocarbon chains pack more tightly, thereby providing more steric hindrance to their conformational dynamics. The tighter packing of both the chains and the headgroups would also impede the flow of lipids within the bilayer, making it less fluid. Such lateral fluidity could also be reduced by increased mini-interdigitation of chains near the bilayer center; this would be brought about because cholesterol is too short to reach the midplane, and chains from the other monolayer could fill the gap. In any case, more ordered structures are generally less fluid, which is typically described in soft matter physics as having higher viscosity. However, even though the zero cholesterol case requires viscosity, as emphasized in connection with Fig. 7, we do not necessarily believe that viscosity increases with cholesterol, as will be discussed next.

6.4 Diffusional softening

The theory in Section 2 is a phenomenological theory that does not explain either the bending modulus or the membrane viscosity in more basic terms. Of course, one would like to understand what affects these phenomenological parameters, so we have extended the phenomenological theory to include the dynamical theory of diffusional softening. Since the bending modulus K_C has to match its equilibrium value, we focus on how diffusional softening affects the viscosity with added cholesterol. Two ways to fit the data with diffusional softening are described in Section 5. Unfortunately, the χ^2 are essentially the same for these two ways and also for not including diffusional softening at all, so we can not report a best result. Nevertheless, it is interesting to compare these three cases in Table 1, which summarizes the 50% cholesterol results. The amount of diffusional softening is quantified by α, and the influence of viscosity is quantified by the ratio of its value at 50% cholesterol to no cholesterol. For equally good fits to these NSE data, one can increase the importance of either one by reducing the importance of the other. This is illustrated in Fig. 10 by the close agreement of the three cases for times less than 300 ns.

Table 1 Values at 50% cholesterol of diffusional softening parameter α, ratio of viscosity to its value at 0% cholesterol and ratio of κ to K_C

Case	Fig.	α	η_{50}/η_0	κ/K_C
1	6	0	5.5	1
2	8	0.24	3.3	1.3
3	9	0.54	1	2.2

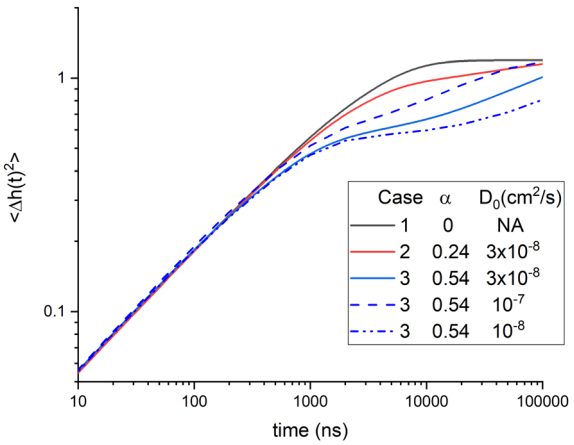

Fig. 10 Long time calculations of $\langle \Delta h^2(t) \rangle$ for cases 1–3 with different values of D_0 for case 3.

Table 1 also compares the results for the theoretical stiffened modulus κ that would pertain if lipid lateral diffusion could be frozen. This might also pertain to short-time NSE dynamics before lipid lateral diffusion occurs, although diffusion begins at time zero, and the early NSE relaxation is dominated by the shortest-length scale modes. Nevertheless, κ is easily obtained from the values of α and the equilibrium K_C *via* eqn (10). A comparison is the inclusion of DOPE in POPC, where, like cholesterol, the small PE headgroup induces a large negative spontaneous curvature. In that case, adding 40% DOPE gave a ratio of about 1.3 for κ/K_C,[11] similar to what is obtained for cholesterol in case 2 in Table 1. Case 3 in Table 1 has a larger value of κ/K_C that is suggestive of the three-fold increase in the bending modulus reported earlier.[6] However, the intrinsic non-softened κ is not the same as the K_{CD} obtained by setting η_m to zero because K_{CD}/K_C is a much larger 8.5 with the addition of 50% cholesterol One might consider using the polymer brush model to extract κ from K_{CD}, but this step has no basis in the theory in Section 2, and it would involve the questionable use of eqn (12) in eqn (11).

It may be noted that a recent simulation shows diffusion of cholesterol that is coupled to undulations.[12] That paper also shows that flip–flop is a parallel pathway to couple cholesterol concentration to undulations, and it reported that the kinetics are faster in DOPC bilayers than in DPPC bilayers, consistent with enabling greater diffusional softening. Incidentally, another recent simulation paper, although not reporting lateral diffusion, also found strongly non-universal effects of cholesterol on the static bending modulus with little change in K_C when cholesterol was added to DOPC.[39]

It is also necessary to appreciate how it is possible that cholesterol increases K_C for DMPC and DPPC, with saturated chains, and not for unsaturated DOPC even though, alone, these PC lipids likely have values of spontaneous curvature that are all small compared to cholesterol or to PE lipids. If diffusion could be suppressed, then cholesterol would increase K_C for both DMPC and DOPC, but likely more for DMPC because cholesterol has a larger effect on the structure of saturated chains.[1,2] Then, diffusional softening would decrease K_C, but the amounts could also be different because it has been argued that the effective spontaneous curvature of lipids in a mixture are non-additive and therefore can be quite different depending upon the other lipid(s).[40]

While Fig. 10 emphasizes that the time regime available to NSE is unlikely to discriminate between the three cases, it suggests that they might be discriminated by their behavior at longer times. However, unsurprisingly, the coefficient of lateral diffusion D_0 also affects the time course of $\langle \Delta h^2(t) \rangle$ as shown for the three case 3 calculations with different values of D_0. It should also be mentioned that the traditional inclusion of compression modes[26,27,29] would also affect the dynamics at longer times, both for pure lipids and for mixtures. That would make it even more difficult to disentangle the parameters involved in diffusional softening. However, such a theory might justify providing experimental values of the neutral surface h if eqn (11) remains valid.

6.5 Comparison of viscosity to literature values

We obtain 0.48 ± 0.1 nPa s m for DOPC. We also find 0.8 ± 0.1 nPa s m for POPC/POPS vesicles but defer a detailed analysis to the authors of this recent study.[7] We should note that these values were obtained using a structural radius R = 30 nm. When we use a larger radius of 40.3 nm for DOPC, we obtain 0.88 nPa s m, so this difference may be a better estimate of our uncertainty. Literature results for membrane viscosity of DOPC bilayers have been reported as low as η_m = 0.15 nPa s m to as high as 16.7 nPa s m as can be seen in the appendix of a recent paper.[41] That paper studied transient deformation of GUVs and reported η_m = 4.11 ± 2.63 nPa s m for DOPC, 7.00 ± 4.77 nPa s m for DOPC : Chol(1 : 1) and 9.32 ± 5.95 nPa s m for POPC. Given the large reported uncertainties, the trends with cholesterol and saturation are consistent with our results, but the values themselves are an order of magnitude larger. Perhaps this could be due to viscosity having a length scale dependence. On the other hand, the largest value of 16.7 nPa s m also came from NSE on small vesicles,[6] but a different protocol and analysis were used, and the deuterated data were different than the protonated data we have reanalyzed. Interestingly, η_m more than doubled with only 20% cholesterol, even more than we report in Fig. 6 and much more than in Fig. 8 when diffusional softening was included. The literature value closest to our DOPC value is 0.59 ± 0.2 nPa s m from probe diffusion in GUVs.[42] Values from smaller vesicles include 0.20 nPa s m,[43] 0.84 nPa s m,[44] and 0.15 nPa s m,[45] and simulations gave 0.197 ± 0.007 nPa s m.[46] It appears that our result for DOPC is closer to these latter values, but we are loathe to discount the

results of the electrodeformation method[41] that clearly observes relaxation on a large length scale. Aside from the magnitudes, it seems likely that there is an increase in η_m with cholesterol but how much is still to be determined.

7 Conclusions

Neutron spin echo provides a valuable but limited time window into the dynamics of lipid bilayers. This limitation and the statistical quality of current NSE data restrict the application of NSE data to determining essentially only one physical quantity. Although NSE practitioners have hitherto focused on obtaining the equilibrium bending modulus,[6,7,13–17,33] this paper maintains that NSE is better suited to obtaining the non-equilibrium viscosity. Importantly, the new phenomenological theory applied to DOPC with no cholesterol requires non-zero viscosity to fit the NSE data and the equilibrium K_C.

For the interesting case of cholesterol in DOPC bilayers, we find that the inclusion of viscosity fits the NSE data better while constraining K_C to the value obtained from equilibrium measurements. This supports the perspective embedded in the phenomenological theory in Section 2 that a single time-independent bending modulus suffices. Our extension of that theory to include diffusional softening allows us to refine how membrane viscosity may change with the addition of cholesterol. While keeping the same equilibrium K_C modulus that does not change when adding cholesterol to DOPC bilayers, the general diffusional softening theory generates a stiffened modulus that has a stiffening factor for 50% cholesterol ranging from 1 to 2.2 for different assumptions that fit the NSE data equally well. Dynamical data at longer times would be required to resolve this ambiguity and, more generally, to determine how much of the effect of cholesterol can be attributed to diffusional softening *versus* changes in membrane viscosity.

Author contributions

J. N. conceptualized the work, F. H. and J. N. analyzed the data and wrote the manuscript.

Data availability

The data were previously published in ref. 6 and were accessed at Virginia Tech's Data Repository (VTechData; DOI: 10.7294/v8w6-7760). The software used for the NSE data analysis shown in the ESI was published in Kirby *et al.*[47]

Conflicts of interest

There are no conflicts to declare.

Acknowledgements

J. N. thanks Markus Deserno and Alex Sodt for discussions of diffusional softening, Michi Nagao and Liz Kelley for NSE discussions, and especially the latter for sending the recent POPC/POPS data and for collaborative fitting of older unpublished data. F. H. acknowledges support from the U.S. Department of Commerce Awards 70NANB17H299 and 70NANB24H248. Certain commercial materials, equipment, and instruments are identified in this work to describe the experimental procedure as completely as possible. In no case does such an identification imply a recommendation or endorsement by NIST, nor does it imply that the materials, equipment, or instruments identified are necessarily the best available for the purpose.

References

1 J. Pan, T. T. Mills, S. Tristram-Nagle and J. F. Nagle, *Phys. Rev. Lett.*, 2008, **100**, 198103.
2 J. Pan, S. Tristram-Nagle and J. F. Nagle, *Phys. Rev. E: Stat., Nonlinear, Soft Matter Phys.*, 2009, **80**, 021931.
3 R. S. Gracia, N. Bezlyepkina, R. L. Knorr, R. Lipowsky and R. Dimova, *Soft Matter*, 2010, **6**, 1472–1482.
4 A. Tian, B. R. Capraro, C. Esposito and T. Baumgart, *Biophys. J.*, 2009, **97**, 1636–1646.
5 B. Sorre, A. Callan-Jones, J.-B. Manneville, P. Nassoy, J.-F. Joanny, J. Prost, B. Goud and P. Bassereau, *Proc. Natl. Acad. Sci. U. S. A.*, 2009, **106**, 5622–5626.
6 S. Chakraborty, M. Doktorova, T. R. Molugu, F. A. Heberle, H. L. Scott, B. Dzikovski, M. Nagao, L.-R. Stingaciu, R. F. Standaert and F. N. Barrera, *et al.*, *Proc. Natl. Acad. Sci. U. S. A.*, 2020, **117**, 21896–21905.
7 R. Granek, I. Hoffmann, E. G. Kelley, M. Nagao, P. M. Vlahovska and A. Zilman, *Eur. Phys. J. E: Soft Matter Biol. Phys.*, 2024, **47**, 12.
8 S. Leibler, *J. Phys.*, 1986, **47**, 507–516.
9 P. V. Bashkirov, P. I. Kuzmin, J. Vera Lillo and V. A. Frolov, *Annu. Rev. Biophys.*, 2022, **51**, 473–497.
10 H. J. Lessen, K. C. Sapp, A. H. Beaven, R. Ashkar and A. J. Sodt, *Biophys. J.*, 2022, **121**, 3188–3199.
11 K. Sapp, M. Aleksanyan, K. Kerr, R. Dimova and A. Sodt, *Phys. Rev. E*, 2023, **107**, 054403.
12 M. Pöhnl, M. F. Trollmann and R. A. Böckmann, *Nat. Commun.*, 2023, **14**, 8038.
13 S. Gupta and G. J. Schneider, *Soft Matter*, 2020, **16**, 3245–3256.
14 B. Brüning, R. Stehle, P. Falus and B. Farago, *Eur. Phys. J. E: Soft Matter Biol. Phys.*, 2013, **36**, 1–8.
15 M. Mell, L. H. Moleiro, Y. Hertle, P. Fouquet, R. Schweins, I. López-Montero, T. Hellweg and F. Monroy, *Eur. Phys. J. E: Soft Matter Biol. Phys.*, 2013, **36**, 1–13.
16 E. G. Kelley, E. E. Blick, V. M. Prabhu, P. D. Butler and M. Nagao, *Front. Phys.*, 2022, **10**, 866024.
17 I. Hoffmann, *Front. Phys.*, 2021, **8**, 620082.
18 M. S. Jablin, K. Akabori and J. Nagle, *Phys. Rev. Lett.*, 2014, **113**, 248102.
19 A. Zilman and R. Granek, *Phys. Rev. Lett.*, 1996, **77**, 4788.
20 N. Kucerka, J. Pencer, J. N. Sachs, J. F. Nagle and J. Katsaras, *Langmuir*, 2007, **23**, 1292–1299.
21 E. Wu, K. Jacobson and D. Papahadjopoulos, *Biochemistry*, 1977, **16**, 3936–3941.

22 N. Kahya, D. Scherfeld, K. Bacia, B. Poolman and P. Schwille, *J. Biol. Chem.*, 2003, **278**, 28109–28115.
23 H. A. Faizi, R. Granek and P. M. Vlahovska, *Proc. Natl. Acad. Sci. U. S. A.*, 2024, **121**, 1–7.
24 B. Kollmitzer, P. Heftberger, M. Rappolt and G. Pabst, *Soft Matter*, 2013, **9**, 10877–10884.
25 I. Hoffmann, C. Hoffmann, B. Farago, S. Prévost and M. Gradzielski, *J. Chem. Phys.*, 2018, **148**, 104901.
26 M. C. Watson, Y. Peng, Y. Zheng and F. L. Brown, *J. Chem. Phys.*, 2011, **135**, 194701.
27 U. Seifert and S. A. Langer, *Biophys. Chem.*, 1994, **49**, 13–22.
28 J. F. Nagle, *Phys. Rev. E*, 2021, **104**, 044405.
29 A. Yeung and E. Evans, *J. Phys. II*, 1995, **5**, 1501–1523.
30 J. F. Nagle, E. A. Evans, P. Bassereau, T. Baumgart, S. Tristram-Nagle and R. Dimova, *Proc. Natl. Acad. Sci. U. S. A.*, 2021, **118**, e2025011118.
31 W. Rawicz, K. C. Olbrich, T. McIntosh, D. Needham and E. Evans, *Biophys. J.*, 2000, **79**, 328–339.
32 M. Mell, L. H. Moleiro, Y. Hertle, I. López-Montero, F. J. Cao, P. Fouquet, T. Hellweg and F. Monroy, *Chem. Phys. Lipids*, 2015, **185**, 61–77.
33 M. Nagao, E. G. Kelley, R. Ashkar, R. Bradbury and P. D. Butler, *J. Phys. Chem. Lett.*, 2017, **8**, 4679–4684.
34 N. Kučerka, S. Tristram-Nagle and J. F. Nagle, *J. Membr. Biol.*, 2006, **208**, 193–202.
35 R. M. Venable, F. L. Brown and R. W. Pastor, *Chem. Phys. Lipids*, 2015, **192**, 60–74.
36 N. Kučerka, J. F. Nagle, J. N. Sachs, S. E. Feller, J. Pencer, A. Jackson and J. Katsaras, *Biophys. J.*, 2008, **95**, 2356–2367.
37 M. Hamm and M. Kozlov, *Eur. Phys. J. E: Soft Matter Biol. Phys.*, 2000, **3**, 323–335.
38 J. F. Nagle, *Chem. Phys. Lipids*, 2017, **205**, 18–24.
39 G. Fiorin, L. R. Forrest and J. D. Faraldo-Gómez, *PNAS nexus*, 2023, **2**, pgad269.
40 A. J. Sodt, R. Venable, E. Lyman and R. Pastor, *Phys. Rev. Lett.*, 2016, **117**, 138104.
41 H. A. Faizi, R. Dimova and P. M. Vlahovska, *Biophys. J.*, 2022, **121**, 910–918.
42 C. Herold, P. Schwille and E. P. Petrov, *Phys. Rev. Lett.*, 2010, **104**, 148102.
43 Y. Nojima and K. Iwata, *J. Phys. Chem. B*, 2014, **118**, 8631–8641.
44 Y. Wu, M. Štefl, A. Olzyńska, M. Hof, G. Yahioglu, P. Yip, D. R. Casey, O. Ces, J. Humpolčková and M. K. Kuimova, *Phys. Chem. Chem. Phys.*, 2013, **15**, 14986–14993.
45 G. Chwastek, E. P. Petrov and J. P. Sáenz, *ChemBioChem*, 2020, **21**, 836–844.
46 A. Zgorski, R. W. Pastor and E. Lyman, *J. Chem. Theory Comput.*, 2019, **15**, 6471–6481.
47 B. J. Kirby, P. A. Kienzle, B. B. Maranville, N. F. Berk, J. Krycka, F. Heinrich and C. F. Majkrzak, Phase-sensitive specular neutron reflectometry for imaging the nanometer scale composition depth profile of thin-film materials, *Curr. Opin. Colloid Interface Sci.*, 2012, **17**, 44–53.